Effect of composition on ductility dip cracking of 690 nickel alloy during multipass welding

A. Rapetti, F. Christien, F. Tancret, P. Todeschini, S. Hendili

Version of Record: https://www.sciencedirect.com/science/article/pii/S2352492819311110
Manuscript_ab73bee1e84d1be359a509a463518dc5

Effect of composition on ductility dip cracking of 690 nickel alloy during multipass welding

A. Rapetti[1,2], F. Christien[3,*], F. Tancret[2], P. Todeschini[1], S. Hendili[4]

[1] EDF R&D, Materials and Mechanics of Components Department, F-77818 Moret-sur-Loing, France

[2] Université de Nantes, Institut des Matériaux Jean Rouxel (IMN), Polytech Nantes, BP 50609, 44306 Nantes Cedex 3, France

[3] Mines Saint-Etienne, Univ Lyon, CNRS, UMR 5307 LGF, Centre SMS, F - 42023 Saint-Etienne, France

[4] EDF R&D, Industrial Risk Management Department, F-78400 Chatou, France

* Corresponding author: Frédéric Christien, frederic.christien@emse.fr, +33 477420018

ABSTRACT

This paper deals with Ductility Dip Cracking (DDC) during multipass welding of 690 filler metals. In addition to industrial alloys (152 and 52M), model alloys of controlled purity were also used to unambiguously demonstrate the effect of elemental sulphur and carbon. The sensitivity of each alloy to DDC was measured with the recently developed Refusion Cracking Test (RCT). It is confirmed that the cracks observed in this study result from DDC, not from liquation nor solidification cracking. DDC cracks are in most cases observed after several welding passes. The detrimental effect of sulphur and beneficial effect of carbon on

the resistance to DDC are clearly evidenced. The good resistance to DDC of the industrial alloys, compared to the model alloys, is related to their niobium content.

KEYWORDS

Ductility Dip Cracking, DDC, Intermediate Temperature Embrittlement, Nickel alloys, Grain boundary segregation, Multipass welding, Model alloys

INTRODUCTION

Nickel based alloys are used in the primary circuit of nuclear Pressurized Water Reactors (PWR) due to their good resistance to corrosion. Nowadays Inconel 690® (~60 wt% Ni, ~30 wt% Cr, ~9–10 wt% Fe and ~0.04 wt% C) is the most used for new components and repair. Welding filler metals for Inconel® 690, like grades 152 and 52M, described later, can be sensitive to Ductility Dip Cracking (DDC), a solid-state cracking phenomenon that occurs in the temperature range of 0.5 to 0.8 of the alloy solidus temperature. [1,2]. DDC manifests itself in intergranular cracks that form in the heat affected zone (HAZ) of previous weld beads during multipass welding operations.

As detailed in the background section of this paper, there is currently no general agreement in the literature on the root cause of DDC in nickel alloys during welding. In particular, it is difficult to identify any clear effect of specific elements like sulphur, carbon or niobium on the DDC. Another difficulty is that various techniques are used to characterise DDC, which give results that are different in nature and difficult to compare to each other. The first part of this paper ("Background" section) reviews the different mechanisms of DDC proposed in the literature and tries to identify some correlations between DDC sensitivity and the chemical composition of 690 alloys. The objective of the experimental work proposed thereafter is notably to clarify the effect of sulphur and carbon on the DDC of 690 alloys. To achieve that, model alloys with controlled compositions were used, in addition to industrial alloys. The sensitivity to DDC of each alloy was determined from the Refusion Cracking Test (RCT) recently developed [3].

BACKGROUND

DDC mechanisms

In the literature, various metallurgical explanations can be found for DDC. Table 1 lists different mechanisms or metallurgical features suspected to have an influence on DDC. The first mechanism listed in Table 1 is grain boundary sliding. Different authors observed signs of grain boundary sliding around DDC cracks [4–8]. They concluded that this phenomenon could be the cause of DDC. However Zheng [9] argued that intergranular sliding cannot by itself be responsible for DDC because high temperatures enhance intergranular sliding, even in cases where DDC is not observed.

Several studies mention an influence of the grain boundary morphology on DDC. It is stated that materials with tortuous grain boundaries are less sensitive than materials with straight ones [1,10–12]. For these authors, tortuosity would better distribute stress along the grain boundaries during welding and reduce the sensitivity to cracking. It is important to note that in the majority of the studies presented in Table 1, the grain boundaries tortuosity is not accurately quantified, nor even defined. Nevertheless, one study reveals that it is possible to design alloys with relatively straight grain boundaries and high resistance to DDC [13]. The suspected beneficial impact of grain boundary tortuosity is most often attributed to niobium. Indeed, several studies show that niobium addition decreases DDC sensitivity [1,2,14–17]. This niobium addition increases the amount of primary carbides, suspected to increase the grain boundary tortuosity.

Secondary carbides are sometimes reported to have an influence on DDC sensitivity. However, there is no consensus on the exact role of those carbides. Indeed, in some cases it is stated that intergranular secondary carbides increase the DDC sensitivity [6,18–22] by cavity formation around carbides during hot deformation. On the contrary, in other cases [6,7,22–24], it is stated that intergranular secondary carbides decrease the DDC sensitivity by limiting

the sliding of grain boundaries. Moreover, as reported by Zheng [9], some alloys without any precipitates show high sensitivity to DDC, which tends to show that secondary carbides are probably not among the main origins of DDC.

Table 1. DDC most documented hypotheses in nickel alloys.

Mechanisms or metallurgical features	*References*
Grain boundary sliding	[4–8]
Grain boundary morphology	[1,10–17,22,25–27]
Secondary carbides increase the sensitivity to DDC	[6,18–22]
Secondary carbides decrease the sensitivity to DDC	[6,7,22–24]
Impurity segregation to grain boundaries	[6,9,28–37]

Grain boundary impurity segregation is the last hypothesis frequently presented in literature. In pure nickel, sulphur segregation decreases grain boundary cohesion and is responsible for ductility loss [32,38]. Similar effects are observed in Fe-36%Ni alloys [30,31]. Several publications show that sulphur increases the DDC sensitivity in nickel-based alloys [6,29,33–35,37].

Correlation between DDC and chemical composition

The sensitivity to DDC has been studied on numerous Inconel 690® filler metals with a nominal composition based on Ni-30Cr-10Fe (wt%) [2,6–8,10,11,14,15,17–19,23–25,27,36,37,39–60]. Those studies were conducted using different experimental methods that we can classify in three types: thermomechanical simulation using fast heating tensile machine tests (using small specimens ~ 50 g), externally loaded welding tests (generally using medium specimens ~ 250 g) and self-restrained welding tests (using large mock-ups ~> 5 kg). In the first class of tests, some studies use thermomechanical simulation tensile tests led to

fracture [7,19,24,39–42] and others use strain to fracture tests (i.e. interrupted tensile tests) [6–8,10,11,17,23,25,27,37,43–52,54]. In the second group of tests, PVR (Programmierter Verformungs Riss) tests [2,15] and Varestraint tests [39,42,55–58] are used to study DDC; in some publications self-restrained tests are used [14,18,36,59,60]. The data obtained from those techniques are different in nature (elongation to fracture, number of cracks, etc.), so their direct comparison is not possible. However, for comparison purposes it is possible to extract from those studies a "DDC-sensitivity factor" ranging from zero to one, where a factor equal to zero corresponds to a minimum of sensitivity among a series of alloys (for example a minimum number of cracks observed at the surface of a Varestraint specimen), whereas a factor equal to one corresponds to a maximum of sensitivity. The factors obtained from different studies can then be put together and relations to composition can be investigated.

Individual studies sometimes conclude on a detrimental role of S and/or P, and/or on a beneficial effect of Nb and/or Mo. If obvious, this should be confirmed as general trends by plotting, in Figure 1, the present DDC sensitivity factor as a function of the "S+P" and "Nb+Mo" contents. The items a), b), c), etc. in Figure 1 correspond to different experimental techniques. In some cases, the S+P or Nb+Mo content is not available, which results in no point in the graphs. In Figure 1 c), only the Nb content is taken into consideration because the Mo content is not mentioned in the paper.

A very clear correlation between DDC sensitivity and the S+P content is evidenced in figure 1 e) showing data from Saida et al. [35]. In contrast no obvious correlation is found in the rest of the figure. Concerning the effect of Nb and Mo, a beneficial effect might be evidenced in figure 1 a) to d) but the experimental points are strongly scattered and the correlation is not systematic. Possible correlations of the sensitivity factor with other elements were also investigated but no correlation was evidenced.

From the data available in the literature it seems difficult to correlate the sensitivity to DDC to alloy composition. One of the reasons is certainly that the data come from different experimental methods so their direct comparison is difficult. In particular, the thermo-mechanical conditions (temperature cycle, deformation, deformation rate, etc.) are very different depending on the testing technique. As DDC is classically believed to be associated to a metallurgical evolution in a temperature range, possibly driven by the strain rate [61], thermo-mechanical kinetic conditions are of primary importance. Another possible reason for the near absence of correlation is that the composition of the alloys gathered in Figure 1 usually differs in several elements, not only one. In that case, the effect of a given detrimental element might be counterbalanced by a beneficial one. This makes it very difficult to evidence a correlation between DDC sensitivity and the content of one particular element from the data available in the literature. In addition, the precision on the trace elements is often not better than 0.01%. This poor precision makes it impossible to take account of trace elements, like sulphur, that can be active at the ppm level. Seeing that simple representations did not show any clear influence of elements on DDC sensitivity, we tried automatic data mining but it did not show any clearer effects. For these reasons, we chose in this work to study model alloys in addition to industrial alloys, in order to investigate the effect of particular elements, here sulphur and carbon, on DDC. The recently developed Refusion Cracking Test (RCT) [3] was used to measure the sensitivity to DDC of the different alloys. This test was chosen for two reasons. First it is close to actual conditions of multipass welding. Second it allows using small specimens, which is critically needed here as only small amounts of model alloys are available.

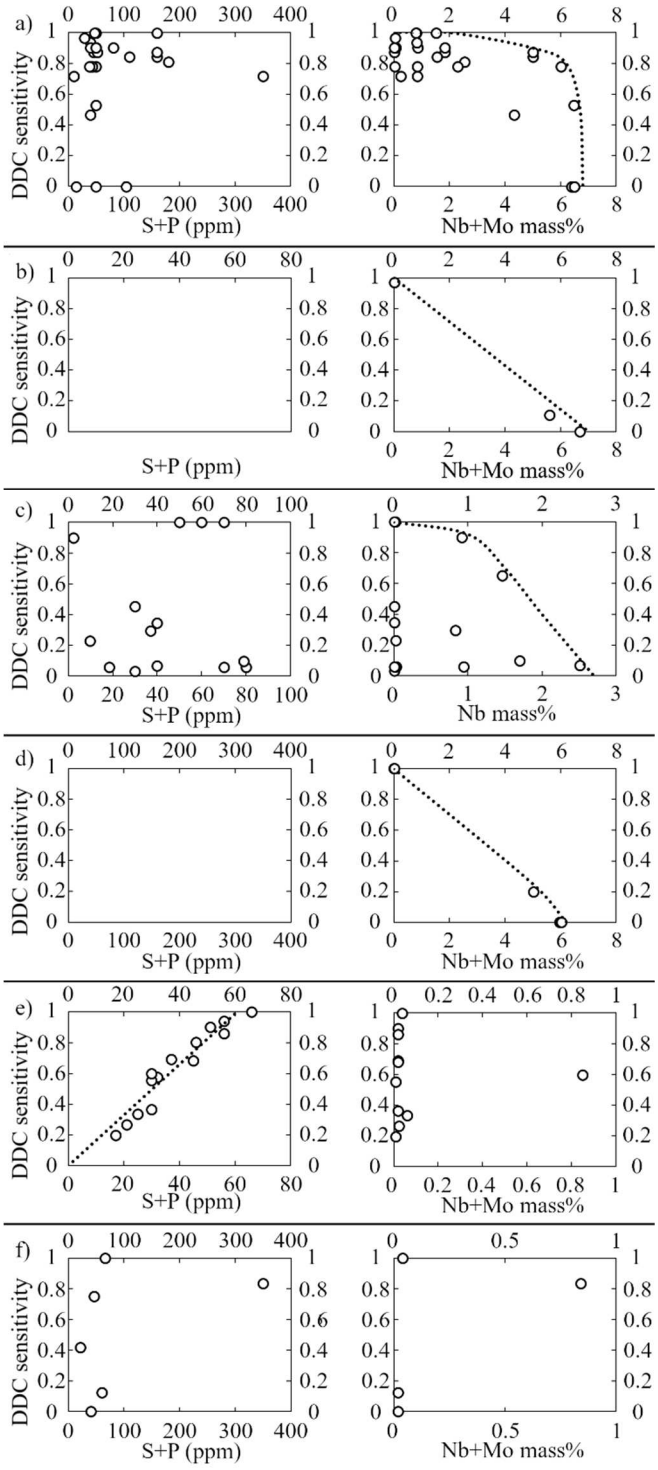

Figure 1. DDC sensitivity as a function of S+P or Nb+Mo content. a) using STF [1,7,17,25,27,49,52] ; b) using in situ STF [51,62] ; c) using Young welding model [14] ; d) using PVR [2,15] ; e) using Varestraint [35] and f) using tensile testing [7,24,42]. The dotted lines are guides for the eyes. Empty graphs result from lack of information.

MATERIALS AND METHODS

Industrial alloys

Two industrial filler metal grades for Inconel® 690, Inconel® filler metal 52M and 152, were studied. Industrial alloys were provided as welded mock-ups (1000×130×60 mm^3 in 2 parts ~64 kg). The mock-ups were obtained by multipass deposition of the fillers, using Gas Tungsten Arc Welding (GTAW) for the 52M filler and Shielded Metal Arc Welding for the 152 filler (Figure 2). In the as-received state, the mock-ups did not show any cracking. It should be mentioned that in this welding configuration, which corresponds to a flat deposition of metal on a flat sheet (without high constraint by a chamfer, or by a particular welding geometry), it is possible, with adjusted parameters, to deposit large quantities of material without cracking, while in contrast industrial welding conditions might lead to cracking. Figure 2 presents the 152-alloy mock-up during manufacturing.

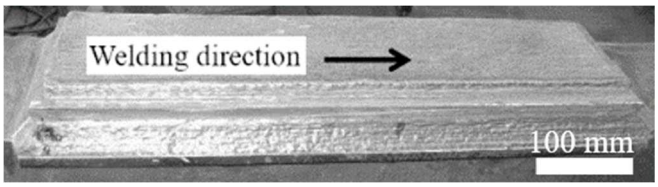

Figure 2. Welded mock-up for 152 alloy during manufacturing.

The composition of the alloys 152 and 52M are given in Table 2 and Table 3.

Table 2. Composition of the industrial alloys used in this study - Major elements (weight %). Cr, Fe, Nb and Mn were measured using X-ray fluorescence. Si, Ti and Al were measured using Glow Discharge Mass Spectrometry (GDMS).

Alloy	Ni	Cr	Fe	Mn	Si	Ti	Al	Nb
52M	Bal.	29.9	8.5	0.75	0.11	0.23	0.11	0.84
152	Bal.	28.7	9.2	3.7	0.51	0.081	0.040	2.1

Table 3. Composition of the industrial alloys used in this study - Residual elements (weight ppm). Carbon was measured using a combustion method. N, O, S, P and Cu were measured using GDMS.

Alloy	C	N	O	S	P	Cu
52M	130	140	30	9.2	17	43
152	370	210	760	51	82	58

Model alloys

Four model alloys based on the composition of our Inconel® filler metal 52M (without niobium) were also studied. These four model alloys were designed in order to test the influence of sulphur and carbon on DDC. The content of all other elements was kept constant.

0.5 kg of each alloy was obtained using vacuum melting in a cold silver crucible. After solidification the four ingots (approximately 25 × 25 × 100 mm) were transformed into plates (7 × 50 × 170 mm) by hammering at room temperature.

Table 4 and Table 5 present the composition of the model alloys. Phosphorus, niobium and copper contents were not measured in the alloys Base + C and Base + CS (with additions of carbon or carbon and sulphur) because they are close to those of the Base alloy due to the manufacturing route.

Table 4. Composition of the model alloys used in this study - Major elements (weight %). All elements were measured using X-ray fluorescence.

Alloy	Ni	Cr	Fe	Mn	Si	Ti	Al
Base	*	29.9	8.42	0.85	0.14	0.21	0.13
Base + C	*	29.7	8.44	0.76	0.11	0.21	0.13
Base + S	*	30.0	8.44	0.84	0.14	0.21	0.13
Base + CS	*	30.0	8.41	0.80	0.14	0.21	0.13

Table 5. Composition of the model alloys used in this study - Residual elements (weight ppm). Nb, Cu and P were measured using GDMS. O, N and C were measured using a combustion method. S was measured using GDMS in Base and Base +C alloys, and using a combustion method in Base + S and Base + CS alloys. NM means "not measured".

Alloy	C	N	O	S	P	Cu	Nb
Base	11	1	7	4.7	1	8	3.3
Base + C	404	1	5	3.1	1	8	3.6
Base + S	16	1	7	52	NM	NM	NM
Base + CS	418	1	4	56	NM	NM	NM

Refusion Cracking Test (RCT)

For this study, the refusion-cracking test (RCT) presented in [3] was used. The RCT is inspired by the multipass welding test developed at EPRI [59] allowing a cyclic loading of the specimen. Nevertheless, it requires only small amounts of material, which makes it possible to investigate the bulk model alloys fabricated for this study, whereas the EPRI test needs large amounts of materials, shaped as filler metal wires or electrodes.

The RCT test simply consists in multiple GTAW passes without filler metal at the surface of a restrained specimen. DDC sensitivity is then estimated through a plot of the total crack length as a function of the number of passes.

Figure 3 presents the experimental setup. The specimen, a 50×40×7mm plate, is GTAW-welded onto a 200×60×6mm steel plate along the red line shown in Figure 3. The steel plate is then clamped as shown in Figure 3 to ensure good mechanical restraint and electrical continuity. The whole is placed in a cylindrical chamber (30 cm in diameter and 7 cm in height). The chamber is filled with argon (< 2 ppm O_2 and < 3 ppm H_2O) during two minutes at 15 $l.min^{-1}$ before each welding pass. Argon is heavier than air and stays mainly at the bottom of the chamber where the oxygen concentration decreases to about 2% (measured using an oximeter located 1 cm from the specimen). This argon-filled-chamber is a complementary protection against oxidation, which is added to the usual protective argon flux from the welding torch.

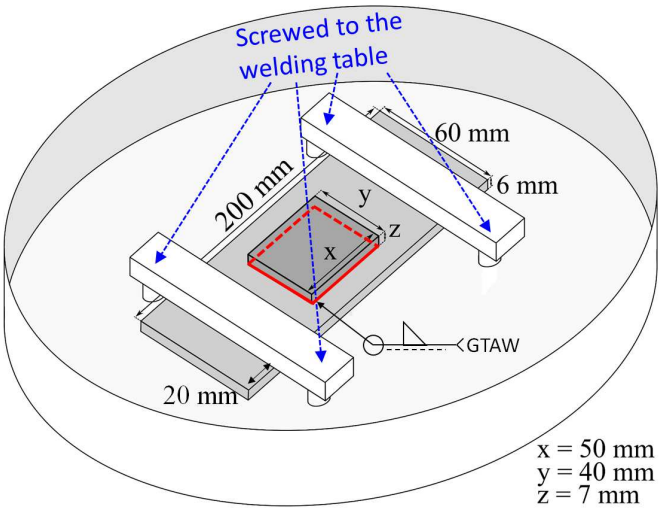

Figure 3. Experimental RCT setup. x, y and z are the specimen dimensions. The specimen is GTAW-welded onto a steel plate along the red line. The clamps are screwed to the welding table.

The specimen surface is mechanically polished and washed with acetone. GTAW welding robot is used at a speed of 11 cm.min^{-1} (1.8 mm.s^{-1}), an intensity of 120 A and a voltage of 10 V. The protective gas is the same as the one used to fill the cylindrical chamber.

Figure 4 presents the fusion lines (i.e. welding beads) positions. Before starting the cracking test itself, two fusion lines are made on the surface, named pre-line A and pre-line B on Figure 4, in order to have a welding solidification structure at specific locations on the specimen. Doing this allows to test alloys with any type of initial microstructure, i.e. in the present case pre-welded mock-ups of as-deposited industrial filler metals or cold-worked bulk model alloys. After that, successive refusion lines are conducted in such a way that their HAZ is located in the melted zone of the two pre-lines. In this way, the welding solidification structure of the pre-lines are cyclically loaded in conditions very representative of a real welding situation.

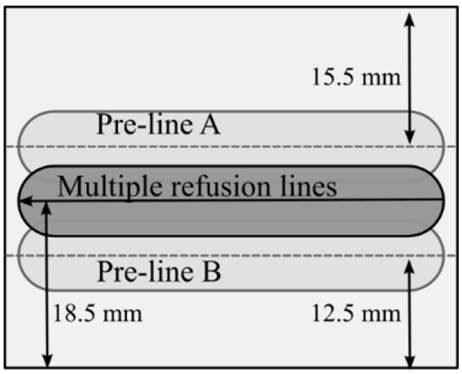

Figure 4. Fusion line positions on the specimen surface during RCT.

After the two pre-lines are made, the specimen surface is mechanically polished and washed with acetone again. After each refusion pass, the surface is washed with acetone. Figure 5 shows the central fusion line with its HAZ. The cracks that develop in the HAZ during the test are schematically represented. The blue rectangle represents a piece of cracked material that was cut to open a crack for fractographic observation (see Results section). The black spots shows the positions of K thermocouples that were spot-welded to the specimen surface after

the pre-lines but before the multiple refusion lines in order to obtain the surface temperature field.

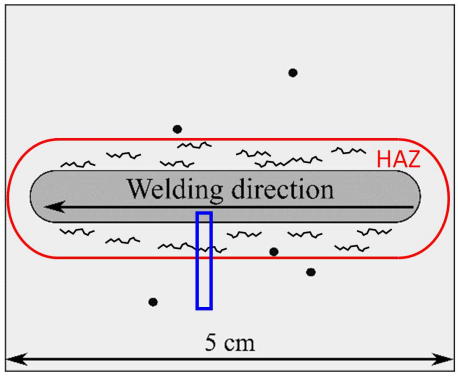

Figure 5. Central fusion line with its HAZ. Schematic representation of the cracks that form in the HAZ during the test. The black dots are examples of thermocouple positions during RCT test (the position of thermocouples can slightly vary from one specimen to another). The blue rectangle represent a small piece of cracked material that was cut to open a crack for fractographic observation.

For each alloy tested, eight refusion passes were conducted with surface observation after each pass, except for model alloy Base + S (only four passes due to severe cracking – see Results section) and for industrial alloy 152 (sixteen passes due to very low cracking occurrence – see Results section – with surface observation after passes 4, 8, 12 and 16). Between passes, high-resolution imaging of the specimen surface over an area of approximately 45 mm × 4 mm was conducted using a binocular magnifier. From the image obtained, the cumulative crack length was measured, as well as the distance of each crack from the edge of the central fusion line. For some specimens, several measurements were conducted on the same image at different times; in that case an error bar representing twice the standard deviation is indicated.

FEM modelling of heat transfers during the RCT test

Finite Element Modelling (FEM) of the heat transfer during the RCT test was conducted using Code_Aster [63] so as to determine the complete temperature field in the specimen at any time. More details about the model can be found in [64]. Figure 6 (a) shows an example of surface temperature field obtained from the model during a pass of the RCT test. The highest temperature zone corresponds to the molten metal. Some input parameters related to the heat source were adjusted in the model to fit the surface temperature measurements obtained from thermocouples. Figure 6 (b) shows the agreement obtained between the calculated and measured time dependence of temperature at different thermocouple locations. Once calibrated, the finite element model was used in this work to determine the maximum temperature reached at observed crack locations. This information is useful to determine the nature of the cracks observed (DDC cracks or liquid cracking).

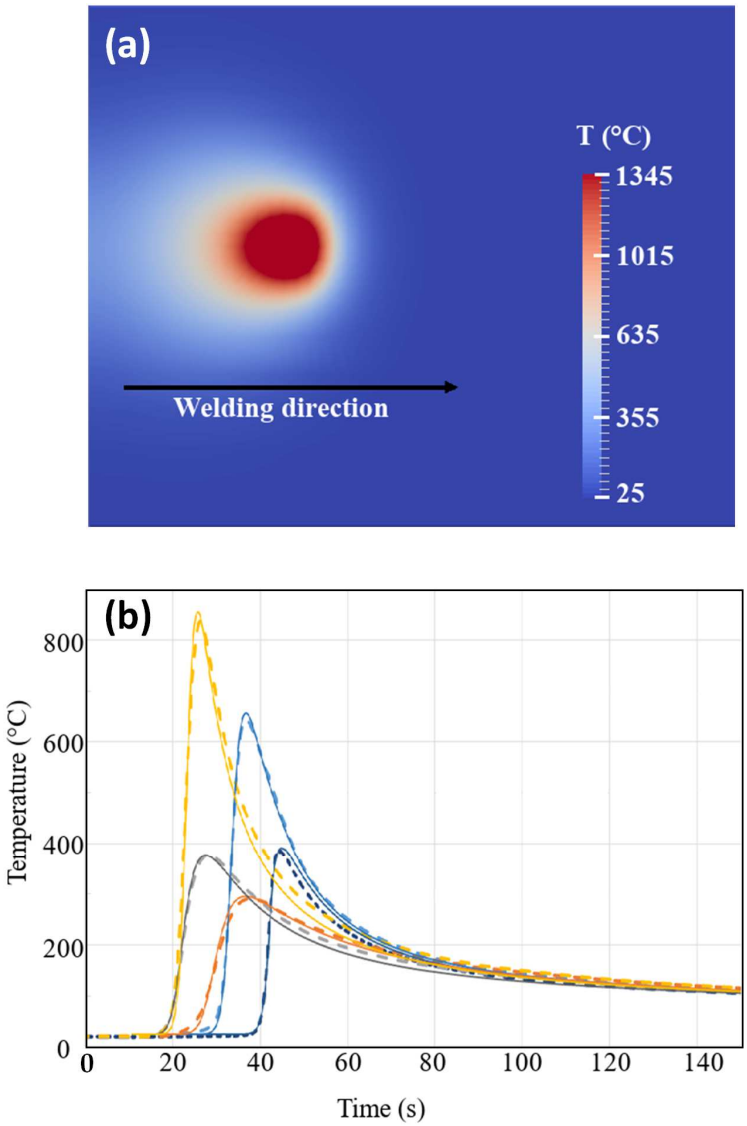

Figure 6. (a): Example of surface temperature field obtained from the model during a pass of RCT test. (b): Agreement obtained between the calculated and measured time dependence of temperature at different thermocouple locations. Dotted lines: measurements. Full lines: simulations.

RESULTS

Figure 7 presents the cumulative crack length obtained using the RCT test on the six alloys tested in this work. The most sensitive alloy is the Base + S model alloy, i.e. the model alloy enriched with sulphur. This alloy is the only one showing cracks after only one pass. After

four passes, the cumulative crack length was so high that the test had to be stopped. The Base model alloy, i.e. with a low carbon content and without any addition of sulphur, behaves far better, which demonstrates the detrimental effect of sulphur. The model alloys containing higher amounts of carbon (Base + C and Base + CS) are less sensitive than the two alloys without addition of carbon whatever the sulphur content is. This demonstrates the beneficial effect of carbon. The two industrial alloys behave better than any of the model alloys. It is interesting to compare for example the 52M and Base + C alloys. Those two alloys have very close composition in major elements, apart from Nb. However, the concentrations of minor elements are different. According to their respective C and S contents, the Base + C alloy (3.1 wt ppm S, 404 wt ppm C) should be more resistant to DDC than the 52M alloy (9.2 wt ppm S, 130 wt ppm C). However, the reverse is observed. A possible explanation is a beneficial effect of niobium (0.84 wt% in 52M, 3.3 wt ppm in Base + C), as often mentioned in literature. The 152 alloy is the one showing the lowest sensitivity: it shows no cracking at all after eight passes, and even after sixteen passes (which is not shown in Figure 7). The C and S contents in the 152 alloy are very close to those in the Base + CS alloy. However, the resistance of the 152 alloy to DDC is far better. Again, this may be due to the high niobium content in that alloy.

Another interesting observation is that a cyclic loading is necessary to observe cracks: apart from the Base + S alloy, cracks are never observed after only one pass. For four of the six alloys tested, at least two to three passes are necessary before any crack is visible.

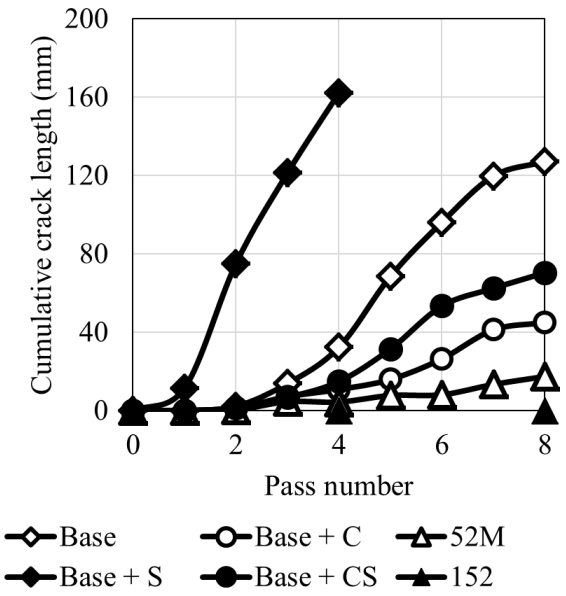

Figure 7. Results of the RCT test for the six alloys studied in this work.

Figure 8 presents the surface observation of a cracked area for model alloy Base + CS from passes 3 to 6. Between pass #3 and pass #4, one crack forms (white arrow) and two others grow (black arrows). From pass #4 to pass #6 it is possible to see that some cracks appear to be geometrically resorbing (black arrows) due to the growth of the big central crack (stress shielding effect [65]).

Figure 9 presents the evolution of a cracked area for model alloy Base + S from passes 2 to 4, showing other examples of cracks observed from the surface, also illustrating the intergranular character of the cracks.

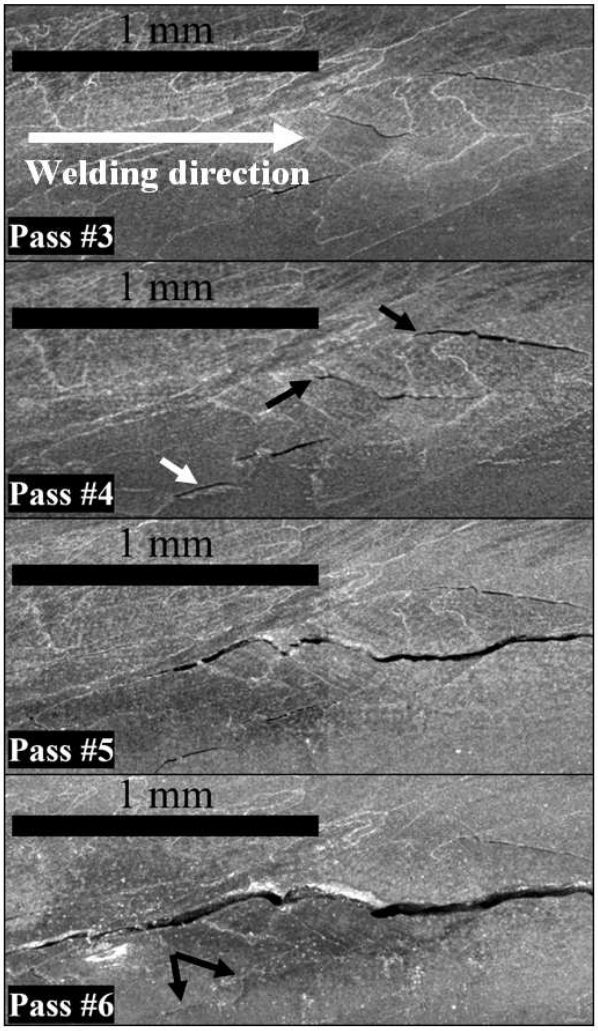

Figure 8. Evolution of a cracked area for model alloy Base + CS from passes 3 to 6.

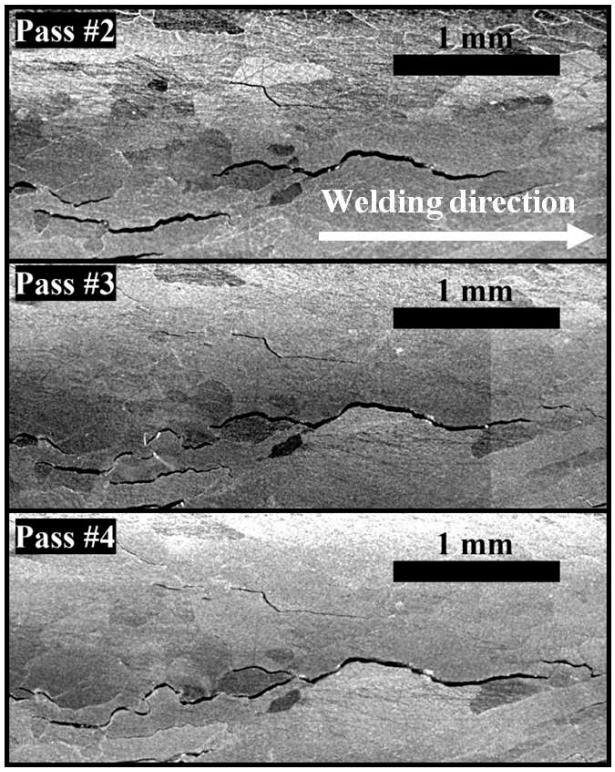

Figure 9. Evolution of a cracked area for model alloy Base + S from passes 2 to 4.

Surface observations have otherwise confirmed that all the cracks are located in the HAZ of the refusion line, corresponding to the melted zone of the pre-lines. No crack is observed in the melted zone of the refusion line. The cracks are oriented approximately parallel to the welding direction, which is consistent with the orientation of the restraint stresses.

Figure 10 presents optical micrographs of Base + CS alloy after eight passes. These observations are obtained after oxalic acid etching. Micrograph a) shows the position of the pre-lines A and B as well as the position of the refusion passes. On micrograph b), the position of the cracks with respect to the fusion line is clearly apparent. It confirms that all the cracks are located in the HAZ of the refusion line. No crack is observed in the melted zone of the refusion line. Micrographs c) and d) confirm the intergranular character of those cracks, also observed on fracture surfaces (Figure 11). In addition it is observed in several places (see arrows in Figure 10 d)) that the crack path is intradendritic. This will be discussed later.

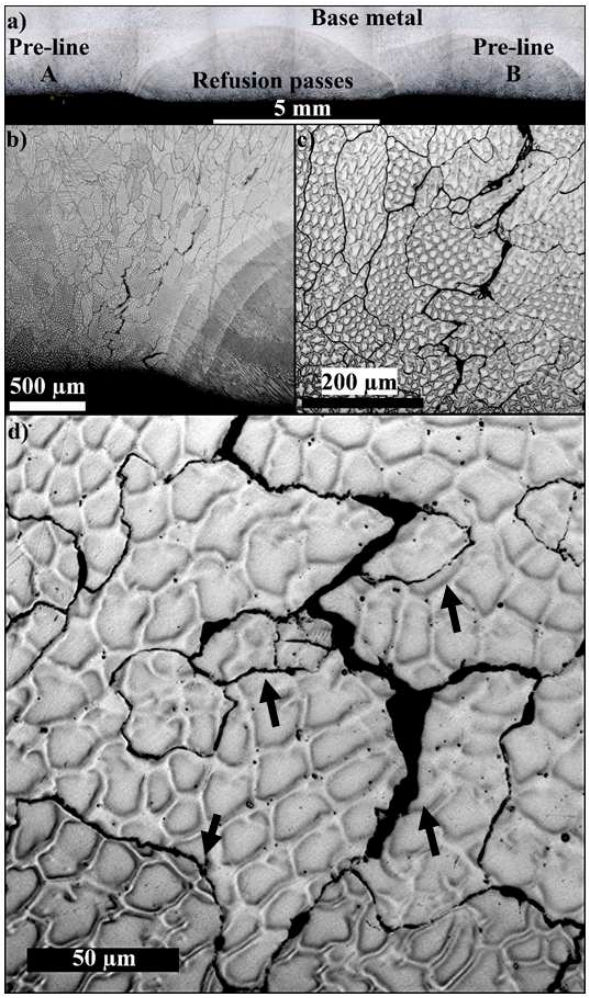

Figure 10. Micrographs of Base + CS model alloy after eight passes. Optical microscopic observations after oxalic acid attack.

Figure 11 presents a Scanning Electron Microscope (SEM) observation of a fracture surface for the Base + S alloy after four passes. This was obtained by cutting, from the RCT specimen, a small piece of material containing a crack (see Figure 5) and opening it by mechanical loading for subsequent fracture surface observation in the SEM. At low magnification (a), the intergranular type of fracture is clearly evidenced. For medium and high magnifications (b and c), the fracture surface appears smooth. Local signs of ductility are observed in rare places (Figure 11 c)), but otherwise cracks mainly appear of brittle nature.

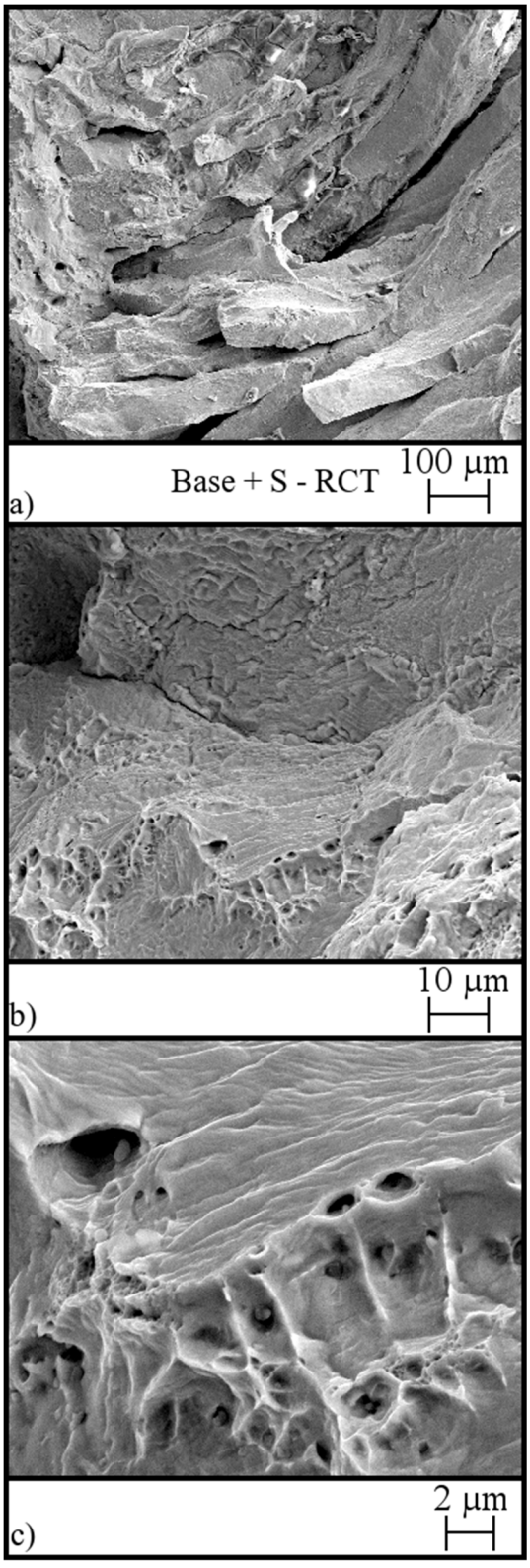

Figure 11. SEM observation of a fracture surface. Base + S alloy after four passes.

Figure 12 shows the maximum surface temperature reached during a pass (T_{max}) on the RCT specimen as a function of the distance to the edge of the refusion line. The black line was

obtained using FEM. The points located below 1000°C correspond to the thermocouple measurements. As expected, the maximum temperature reached during a pass decreases when the distance to the refusion line increases. Good agreement is found between the FEM calculation and the temperature measurements. The points located on the edge of the refusion line correspond to the melting (solidus) temperature of 52M measured using calorimetry (1 354°C). The maximum temperatures (T_{max}) values of the cracking zone are given in Table 6 for the different alloys.

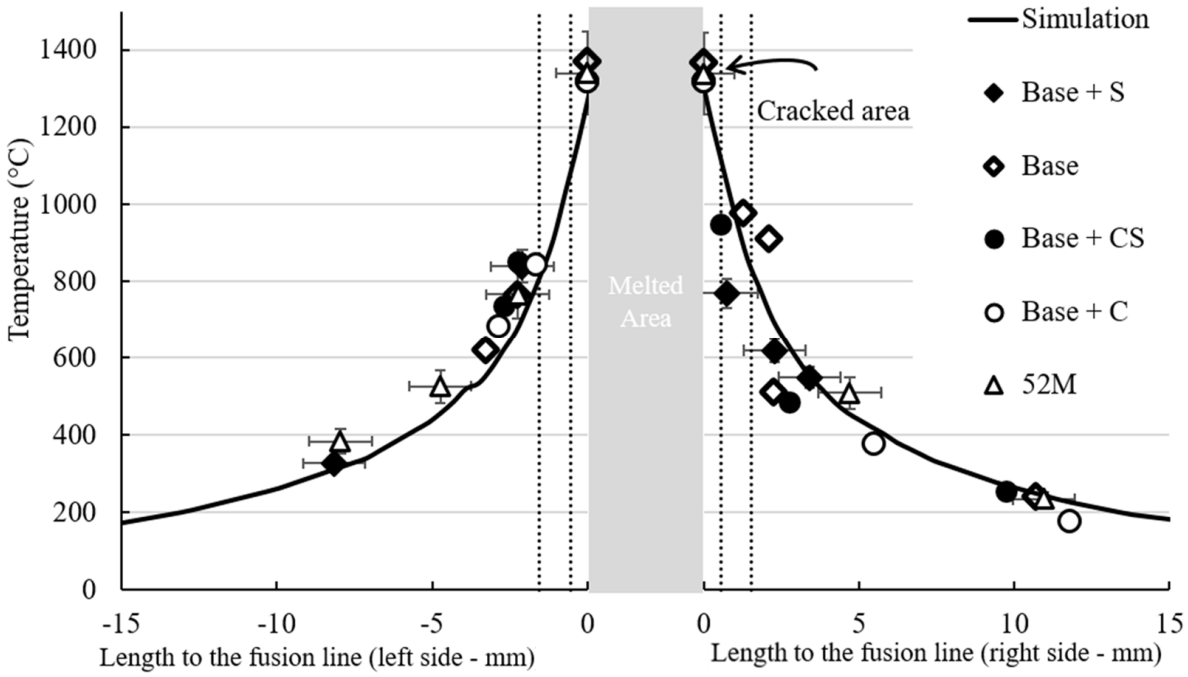

Figure 12. Maximum surface temperature reached during a pass on the RCT specimen as a function of the distance to the edge of the refusion lines for the different alloys (alloy 152 is not considered here as no crack was observed on that alloy). See text for the signification of lines and points.

Table 6. T_{max} values (°C) reached for observed cracks after the fourth pass. (1): T_{max} corresponding to the closest crack; (2): T_{max} corresponding to the farthest crack.

	Base + S	*Base*	*Base + CS*	*Base + C*	*52M*
(1)	1190	1037	1097	1223	1028
(2)	811	750	828	927	839

Most of the cracks are located in a zone where the T_{max} value is in the range 800 to 1200°C. Table 7 shows the liquidus and solidus temperatures of the different alloys obtained from Differential Thermal Analysis (DTA) and/or thermodynamic simulation using MatCalc software and MC_Ni2.011 database. T_{max} values in the cracking area are in all cases below the solidus temperature. For the cracks located far from the refusion lines, T_{max} can be as low as 750°C (for the Base alloy), which is lower than the solidus temperature by approximately 600°C. In addition, it should be noted that T_{max} does not represent here the actual cracking temperature but an upper limit of it. It may then be that the actual cracking temperatures are below the values presented in Table 6.

Table 7. Solidus (T_S) and liquidus (T_L) temperatures of the different alloys obtained from DTA measurements and MatCalc calculations. Equilibrium calculations are processed with the thermodynamic database MC_Ni2.011 with the following elements: Ni, Cr, Fe, Mn, Nb, Al, Ti, Si, C, N.

	DTA measurement		**MatCalc® calculation**			
Alloy	152	52M	152	52M	Base + C	Base
T_L (°C)	1335	1377	1335	1374	1380	1382
T_S (°C)	1272	1354	1247	1330	1320	1370
$T_L - T_S$ (K)	69	23	86	44	60	12

DISCUSSION

Cracking mechanism: DDC or liquid cracking?

The nature of the cracks obtained using the RCT test is to be characterised as it could be questioned whether the cracks are the result of liquid cracking or DDC. However, several arguments can be put forward for DDC cracking rather than liquid cracking. First it is observed that the cracks form only in the HAZ of the refusion line. No crack at all is observed in the refusion line itself. The maximum temperature range of the cracking zone is approximately from 800 to 1200°C which is always below the solidus temperature of any alloy tested. Occasionally some cracks can even be observed in places where the temperature never exceeds 750°C, which is approximately 600°C below the solidus temperature. It is then likely that the material is completely solid when the cracks form. The second argument is based on the cracking path through the microstructure. The cracking is clearly intergranular as shown by several types of observations (Figure 9, Figure 10 and Figure 11). However, the grain boundaries are not necessarily located in interdentritic spaces here because of grain

boundary migration after solidification. It is shown in several locations in Figure 10 (see arrows) that the cracks can go through dentrite arms. So the cracking observed here is intergranular, but not necessarily interdendritic. The third argument is based on the respective behaviour of alloys 52M and 152 during RCT. It was observed that alloy 52M is more sensitive than alloy 152. If the sensitivity was the result of liquid cracking, the reverse should be obtained as alloy 152 is expected to be more sensitive to liquid cracking since its difference between liquidus and solidus temperatures is much larger than for alloy 52M (see Table 7). Finally, the fractographs do not suggest a liquid cracking mechanism. Complementary fracture tests [64] were conducted on tensile specimens of the same materials at temperatures above the solidus to promote liquid cracking. The fracture surfaces obtained were clearly interdendritic and very different from those obtained here. For all these reasons it is concluded that DDC is the cracking mechanism active in the RCT tests conducted in this study.

Effect of sulphur, carbon and niobium

The results shown in Figure 7 were used to relate the material composition to the sensitivity to DDC, estimated here as the crack length obtained after eight passes of RCT. For one of the alloy (Base + S), only four RCT passes were conducted and a sigmoid extrapolation was used to determine the crack length after eight passes. The effect of sulphur, carbon and niobium were considered. Sulphur was found to be the only detrimental element and it is assumed that no crack would be obtained during RCT in the absence of sulphur. Carbon and niobium were considered beneficial and assumed to mitigate the detrimental effect of sulphur. The correlation equation (Eq. 1) was designed to fulfil these conditions.

$$L = \frac{S^n}{a + b \times C + c \times Nb} \qquad 1.$$

where L is the crack length in mm after eight passes of RCT. S, C and Nb are the sulphur, carbon and niobium contents (expressed in wt ppm for S and C, in wt% for Nb). n, a, b and c are fitting parameters.

The four fitting parameters of Eq. 1 were adjusted to obtain the best possible fit of experimental measurements, ($n = 0.2604$, $a = 0.0108$, $b = 6.64\ 10^{-5}$, $c = 0.1570$) which is plotted in Figure 13.

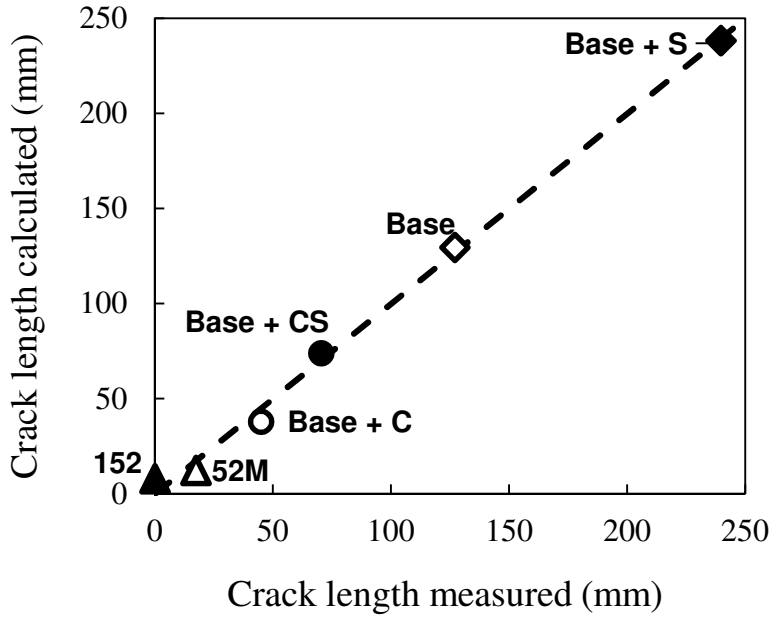

Figure 13. Predicted crack length after eight passes of RCT (using Eq. (1)) vs measured values.

The results clearly show a detrimental effect of sulphur, which is consistent with other studies [6,29,33–35,37]. It is inferred that sulphur segregates to the grain boundaries during the RCT test. Sulphur is indeed known to weaken the metal bonds in grain boundaries in nickel alloys [31,66,67]. As mentioned earlier, in five of the six materials studied here, several passes are needed before cracks can be observed. A possible explanation would be a dynamic sulphur-assisted crack propagation [61]. To be observable, a crack must grow to a certain length (of

the order of 100 µm). This requires a certain time spent under tensile stress so that the crack can grow. It appears that this time exceeds one single pass for five of the six materials tested here. In other words, several passes are needed before a crack can be observed. Of course, this time depends on the average crack growth rate, that itself depends on the material composition, including sulphur concentration. This is notably related to the kinetics of sulphur grain boundary segregation during the pass. It appears that the crack growth rate in the Base + S alloy is high enough to obtain observable cracks after only one pass, which is not the case for the other alloys.

In contrast to sulphur, carbon is found to be beneficial. Carbon is present in solid solution and as carbides. Figure 14 shows the phase equilibrium diagrams obtained from Matcalc® for the Base and Base + C alloys. For the Base + C alloy containing 400 wt ppm of carbon, $Cr_{23}C_6$ carbides are expected in the temperature range of cracking (~800 - 1200°C) at a level of approximately 1 wt % (phase fraction). This would be consistent with a possible beneficial effect of intergranular carbides as proposed by Nissley and Lippold [23] or Chen et al. [7]. However, the beneficial effect of carbon may also be related to its presence in the austenite solid solution. Thermodynamic calculations show that the equilibrium concentration of dissolved carbon at 900°C is larger by approximately a factor of ten in the Base + C alloy than in the Base alloy. The beneficial effect may derive from a thermodynamic and/or kinetic competition in segregation of carbon or sulphur [68] to the grain boundaries. Further research would be needed to clarify the exact behaviour of carbon. The RCT tests conducted on the two industrial materials (containing niobium) show that those materials are more resistant to DDC than any of the model alloys tested. These observations are consistent with the beneficial effect of niobium mentioned in the literature [1,2,14–17]. The question of a possible relation between niobium and grain boundary tortuosity was not investigated in this work and would need further clarification [1,10–13].

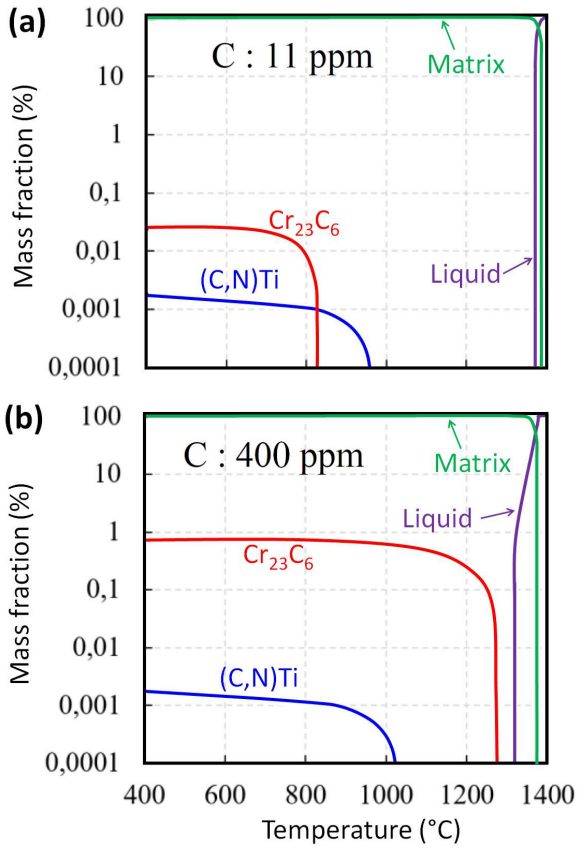

Figure 14. Phase equilibrium diagrams for model alloy. (a): Base, (b) : Base + C. Calculated with MatCalc. The considered phases are liquid, FCC matrix, $Cr_{23}C_6$ carbides and (C,N)Ti.

CONCLUSIONS

This paper presents new results on Ductility Dip Cracking during welding of nickel alloys of the Inconel 690 family, obtained using the Refusion Cracking Test. This self-restraint test with multiple fusion lines presents several advantages: it does not require a large amount of material, it is close to actual multi-pass welding conditions and is easy to perform. This test was conducted on a series of materials including both model alloys and industrial alloys. The main results can be summarised as follows:

- The RCT method is able to characterise the sensitivity to DDC, that was found very different depending on the alloys tested in this work.
- It was confirmed that the cracks obtained are the result of DDC, not liquid cracking.
- In most cases, several welding passes were needed to observe cracks.
- Sulphur increases the sensitivity to DDC whereas carbon and niobium reduce it.
- A four parameter equation taking account of the sulphur, carbon and niobium content is proposed to describe the results obtained with the RCT test.
- Further research is needed to identify more clearly the metallurgical mechanisms underlying the detrimental or beneficial effect of S, C and Nb.

ACKNOWLEDGMENT

This research was mainly funded by EDF (Electricité de France) with the support of ANRT (Association Nationale Recherche Technologie).

DATA AVAILABILITY STATEMENT

The raw and processed data required to reproduce these findings are available from the corresponding author upon request.

REFERENCES

[1] S.D. Kiser, R. Zhang, B.A. Baker, A New Welding Material for Improved resistance to Ductility Dip Cracking, in: Proceedings of the 8th International Conference on Trends in Welding Research, Pine-Mountain, 2008: pp. 639–644. https://doi.org/10.1361/cp2008twr639.

[2] K. Yushchenko, V. Savchenko, N. Chervtakov, A. Zvyagintseva, E. Guyot, Comparative hot cracking evaluation of welded joints of alloy 690 using filler metals INCONEL 52 and 52MSS, Welding in the World. 55 (2011) 28–35. https://doi.org/10.1007/BF03321317.

[3] A. Rapetti, P. Todeschini, S. Hendili, F. Christien, F. Tancret, A Study of Ductility Dip Cracking of Inconel 690 Welding Filler Metal: Development of a Refusion Cracking Test, in: Proceedings of the ASME 2017 Pressure Vessels and Piping Conference. Volume 6B: Materials and Fabrication., ASME, Waikoloa, Hawaii, USA, 2017: p. V06BT06A022. https://doi.org/10.1115/PVP2017-65348.

[4] Y.C. Zhang, H. Nakagawa, F. Matsuda, Weldability of Fe-36%Ni Alloy (Report VI), Transactions of JWRI. 14 (1985) 325–334.

[5] A. Eilers, J. Nellesen, R. Zielke, W. Tillmann, Analysis of the ductility dip cracking in the nickel-base alloy 617mod, IOP Conference Series: Materials Science and Engineering. 181 (2017) 012020. https://doi.org/10.1088/1757-899X/181/1/012020.

[6] A.J. Ramirez, J.C. Lippold, High temperature behavior of Ni-base weld metal Part II. Insight into the mechanism for ductility dip cracking, Materials Science and Engineering A. 380 (2004) 245–258. https://doi.org/10.1016/j.msea.2004.03.075.

[7] J.Q. Chen, H. Lu, W. Cui, J.M. Chen, Y.F. Huang, Effect of grain boundary behaviour on ductility dip cracking mechanism, Materials Science and Technolgy. 30 (2014) 1189–1196. https://doi.org/10.1179/1743284713Y.0000000431.

[8] E.A. Torres, F.G. Peternella, R. Caram, A.J. Ramirez, In Situ Scanning Electron Microscopy High Temperature Deformation Experoments to Study Ductility Dip Cracking of Ni-Cr-Fe Alloys, in: In-Situ Studies with Photons, Neutrons and Electrons Scattering, Springer, 2010: pp. 27–39.

[9] L. Zheng, G. Schmitz, Y. Meng, R. Chellali, R. Schlesiger, Mechanism of Intermediate Temperature Embrittlement of Ni and Ni-based Superralloys, Critical Reviews in Solid State and Materials Sciences. 37 (2012) 181–214. https://doi.org/10.1080/10408436.2011.613492.

[10] M.G. Collins, J.C. Lippold, An Investigation of Ductility Dip Cracking in Nickel-Based Filler Materials - Part I, Welding Journal. 80 (2003) 288s–294s.

[11] A.J. Ramirez, J.C. Lippold, High temperature behavior of Ni-base weld metal Part I. Ductility and microstructural characterization, Materials Science and Engineering A. 380 (2004) 259–271. https://doi.org/10.1016/j.msea.2004.03.074.

[12] J. Unfried-Silgado, A.J. Ramirez, Modeling and Characterization of As-Welded Microstructure of Solid Solution Strengthened Ni-Cr-Fe Alloys Resistant to Ductility-Dip Cracking Part I : Numerical modeling, Metals and Materials International. 20 (2014) 297–305. https://doi.org/10.1007/s12540-014-1023-z.

[13] C. Fink, J.C. Lippold, A.T. Hope, S. McCracken, Elevated temperature cracking resistance of Ta-Beraing high chromium Ni-base filler metals, in: Proceedings of the ASME 2017 Pressure Vessels and Piping Conference. Volume 6B: Materials and Fabrication., ASME, Waikoloa, Hawaii, USA, 2017: p. V06BT06A029. https://doi.org/10.1115/PVP2017-66130.

[14] G.A. Young, T.E. Capobianco, R.A. Etien-III, J.V. Mullen, S. Leveillee, P.C. Sander, Development of a highly weldable and corrosion resistant nickel-chormium filler metal,

in: 13th Conference on Environmental Degradation of Materials in Nuclear Power Systems, 2007: pp. 1–23.
[15] G. Tirand, C. Primault, V. Robin, Sensibilité à la fissuration à chaud des alliages base nickel à haute teneur en chrome, Matériaux & Techiniques. 102 (2014) 403-1-403–5. https://doi.org/10.1051/mattech/2014035.
[16] W. Mo, S. Lu, D. Li, Y. Li, Effects of filler metal composition on the microstructure and mechanical properties for ER NiCrFe-7 multi-pass weldments, Materials Science and Engineering A. 582 (2013) 326–337. https://doi.org/10.1016/j.msea.2013.06.038.
[17] J.C. Lippold, N.E. Nissley, Further investigations of ductility-dip cracking in high chromium Ni-base filler metals, Welding in the World. 51 (2007) 24–30. https://doi.org/10.1007/BF03266597.
[18] G.A. Young, T.E. Capobianco, M.A. Penik, B.W. Morris, J.J. McGee, The Mechanism of Ductility Dip Cracking in Nickel-Chromium Alloys, Welding Journal. 87 (2008) 31s–43s.
[19] F.F. Noecker, J.N. DuPont, Metallurgical Investigation into Ductility Dip Cracking in Ni-Based Alloys: Part II, Welding Journal. 88 (2009) 62s–77s.
[20] W. Mo, S. Lu, D. Li, Y. Li, Effects of M23C6 on the High-Temperature Performance of Ni-Based Welding Material NiCrFe-7, Metallurgical and Materials Transaction A. 45A (2014) 5114–5126. https://doi.org/10.1007/s11661-014-2439-2.
[21] X. Wei, M. Xu, Q. Wang, M. Zhang, W. Liu, J. Xu, J. Chen, H. Lu, C. Yu, Effect of local texture and precipitation on the ductility dip cracking of ERNiCrFe-7A Ni-based overlay, Materials and Design. 110 (2016) 90–98. https://doi.org/10.1016/j.matdes.2016.07.130.
[22] C. Fink, An investigation on ductility-dip cracking in the base metal heat-affected zone of wrought nickel base alloys—part I: metallurgical effects and cracking mechanism, Welding in the World. 60 (2016) 939–950. https://doi.org/10.1007/s40194-016-0370-4.
[23] N.E. Nissley, J.C. Lippold, Ductility-Dip Cracking Susceptibility of Nickel-Based Weld Metals Part 2 : Microstructural Characterization, Welding Journal. 88 (2009) 131s–140s.
[24] F.F. Noecker, J.N. DuPont, Metallurgical Investigation into Ductility Dip Cracking in Ni-Based Alloys: Part I, Welding Journal. 88 (2009) 7s–20s.
[25] K. Kadoi, T. Uegaki, K. Shinozaki, M. Yamamoto, New measurement technique of ductility curve for ductility-dip cracking susceptibility in Alloy 690 welds, Materials Science and Engineering A. 672 (2016) 59–64. https://doi.org/10.1016/j.msea.2016.06.062.
[26] C. Hua, H. Lu, C. Yu, J.-M. Chen, X. Wei, J.-J. Xu, Reduction of ductility-dip cracking susceptibility by ultrasonic-assisted GTAW, Journal of Material Processing Technology. 239 (2017) 240–250. https://doi.org/10.1016/j.jmatprotec.2016.08.018.
[27] A.T. Hope, J.C. Lippold, Development and testing of a high-chromium, Ni-based filler metal resistant to ductility dip cracking and solidification cracking, Welding in the World. 61 (2017) 325–332. https://doi.org/10.1007/s40194-016-0417-6.
[28] S. Yamaguchi, H. Kobayashi, T. Matsumiya, S. Hayami, Effect of minor elements of hot workability of nickel-base superalloys, Metals Technology. 6 (1979) 170–175. https://doi.org/10.1179/030716979803276110.
[29] F. Matsuda, H. Nakagawa, S. Minehisa, N. Sakabata, A. Ejima, K. Nohara, Weldability of Fe-36% Ni Alloy (Report II), Transactions of JWRI. 13 (1984) 69–75.
[30] L. Ben Mostefa, G. Saindrenan, M.P. Solignac, J.P. Colin, Effect of interfacial sulfur segregation on the hot ductility drop of Fe□Ni36 alloys, Acta Metallurgica et Materialia. 39 (1991) 3111–3118. https://doi.org/10.1016/0956-7151(91)90044-2.

[31] M.T. Perrot-Simonetta, A. Kobylanski, Influence of Trace Elements on Hot Ductility of an Ultra High Purity Invar Alloy, Le Journal de Physique IV. 05 (1995) C7-323-C7-334. https://doi.org/10.1051/jp4:1995739.
[32] G. Saindrenan, R. Le Gall, F. Christien, XV. Propriétés Mécaniques, in: Génie des matériaux: endommagement interfacial des métaux : ségrégation interfaciale et conséquences, Ellipses, Paris, 2002: pp. 181–222.
[33] K. Nishimoto, K. Saida, H. Okauchi, Microcracking in multipass weld metal of alloy 690 Part 1 – Microcracking susceptibility in reheated weld metal, Science and Technology of Welding and Joining. 11 (2006) 455–461. https://doi.org/10.1179/174329306X94291.
[34] H. Okauchi, Y. Nomoto, H. Ogiwara, K. Saida, K. Nishimoto, Metallurgical mechanism of ductility-dip cracking in multipass welds of alloy 690, Transaction of JWRI. 39 (2010) 221–223.
[35] K. Saida, Y. Nomoto, H. Okauchi, H. Ogiwara, K. Nishimoto, Influences of phosphorus and sulphur on ductility dip cracking susceptibility in multipass weld metal of alloy 690, Science and Technology of Welding and Joining. 17 (2012) 1–8. https://doi.org/10.1179/1362171810Y.0000000004.
[36] T.E. Capobianco, M.E. Hanson, Auger Spectroscopy Results from Ductility Dip Cracks Opened Under Ultra-High Vacuum, in: 7th International Conference on Trends in Welding Research, ASM International, Callaway Gardens, 2005: pp. 767–772.
[37] M.G. Collins, A.J. Ramirez, J.C. Lippold, An Investigation of Ductility-Dip Cracking in Nickel-Based Weld Metals - Part III, Welding Journal. 83 (2004) 39s–49s.
[38] T. Miyahara, K. Stolt, D.A. Reed, H.K. Birnbaum, Sulfur segregation on nickel, Scripta Metallurgica. 19 (1985) 117–121. https://doi.org/10.1016/0036-9748(85)90276-5.
[39] M.J. Cola, D.F. Teter, Optical and Analytical Electron Microscopy of Ductility-Dip Cracking In Ni-base Filler Metal 52 - Intial Studies, in: 5th International Conference on Trends in Welding Research, Callaway Gardiens Resort Pine Mountain, Georgia, 1998: pp. 1–6.
[40] S.J. Norton, Development of a Gleeble based test for post weld heat treatment cracking in nickel alloys, Master thesis, Graduate School of The Ohio State University, 2002.
[41] V.R. Davé, M.J. Cola, M. Kumar, A.J. Schwartz, G.N.A. Hussen, Grain Boundary Character in Alloy 690 and Ductility-Dip Cracking Susceptibility, Welding Journal. 83 (2004) 1s–5s.
[42] K. Nishimoto, K. Saida, H. Okauchi, Microcracking in multipass weld metal of alloy 690 Part 2 – Microcracking mechanism in reheated weld metal, Science and Technology of Welding and Joining. 11 (2006) 462–470. https://doi.org/10.1179/174329306X94309.
[43] N.E. Nissley, Development of the strain-to-fracture test to study ductility-dip cracking in austenitic alloys, Master thesis, Graduate School of The Ohio State University, 2002.
[44] M.G. Collins, A.J. Ramirez, J.C. Lippold, An Investigation of Ductility Dip Cracking in Nickel-Based Weld Metals - Part II, Welding Journal. 82 (2003) 348s–354s.
[45] N.E. Nissley, J.C. Lippold, Development of the Strain-to-Fracture Test, Welding Journal. 82 (2003) 355s–364s.
[46] A.J. Ramirez, J.C. Lippold, New Insight into the Mechanism of Ductility-Dip Cracking in Ni-base Weld Metals, in: Hot Cracking Phenomena in Welds, Springer, 2005: pp. 19–41.
[47] N.E. Nissley, Intermediate temperature grain boundary embrittlement in nickel-base weld metals, Phd dissertation, Graduate School of The Ohio State University, 2006. https://etd.ohiolink.edu/.

[48] A.J. Ramirez, J.W. Sowards, J.C. Lippold, Improving the ductility-dip cracking resistance of Ni-base alloys, Journal of Material Processing Technology. 179 (2006) 212–218. https://doi.org/10.1016/j.jmatprotec.2006.03.095.
[49] J.C. Lippold, N.E. Nissley, Ductility-Dip Cracking in High Chromium, Ni-Base Filler Metals, in: Hot Cracking Phenomena in Welds II, Springer, 2008: pp. 409–425.
[50] N.E. Nissley, J.C. Lippold, Ductility-Dip Cracking Susceptibility of Nickel-Based Weld Metals Part 1 : Strain-to-Fracture Testing, Welding Journal. 87 (2008) 257s–264s.
[51] J.S. Unfried, E.A. Torres, A.J. Ramirez, In Situ Observation of Ductility-Dip Cracking Mechanism in Ni-Cr-Fe Alloys, in: Hot Cracking Phenomena in Welds III, Springer, 2011: pp. 295–315. https://doi.org/10.1007/978-3-642-16864-2_15.
[52] R. Qin, H. Wang, G. He, Investigation on the Microstructure and Ductility-Dip Cracking Susceptibility of the Butt Weld Welded with ENiCrFe-7 Nickel-Base Alloy-Covered Electrodes, Metallurgical and Materials Transactions A. 46 (2015) 1227–1236. https://doi.org/10.1007/s11661-014-2699-x.
[53] C. Fink, M. Zinke, S. Jüttner, An investigation of ductility-dip cracking in the base metal heat-affected zone of wrought nickel base alloys—part II: correlation of PVR and STF results, Welding in the World. 60 (2016) 951–961. https://doi.org/10.1007/s40194-016-0352-6.
[54] V.V.C. Kreuter, J.C. Lippold, Ductility-Dip Cracking Susceptibility of Commercially Pure Ni and Ni-Base Alloys Utilizing the Strain-to-Fracture Test, in: Cracking Phenomena in Welds IV, Th. Boellinghaus et al., 2016: pp. 145–159. 10.1007/978-3-319-28434-7_8.
[55] W. Wu, C.H. Tsai, Hot Cracking Susceptibility of Fillers 52 and 82 in Alloy 690 Welding, Metallurgical and Materials Transaction A. 30 (1999) 417–426. https://doi.org/10.1007/s11661-999-0331-2.
[56] J.M. Kikel, D.M. Parker, Ductility Dip Cracking Susceptibility of Inconel Filler Metal 52 and Inconel Alloy 690, in: International Conference on Trends in Welding Research : Pine Mountain GA, 1998: pp. 1–19. https://doi.org/10.2172/661678.
[57] T. Ogura, Y. Morikawa, K. Saida, Evaluation of Ductility-Dip Cracking Susceptibility in Alloy 690 Laser Multipass Weld Metal by Varestraint Test, 34 (2016) 181–188. https://doi.org/10.2207/qjjws.34.181.
[58] S. McCracken, J.C. Lippold, A.T. Hope, T.C. Luskin, B.J. Sutton, B.T. Alexandrov, Welding and Repair Technology Center : Evaluation of High-Chromium Nickel-Base Welding Alloys, Electric Power Research Institute, Palo Alto, CA, 2013.
[59] S. McCracken, J. Tatman, T. Matsuoka, D. Abe, S. Masuda, Welding and Repair Technology Center : Screening Test for High-Chromium Nickel-Base Weld Metals - Preliminary Studies, Electric Power Research Institute, Palo Alto, CA, 2015.
[60] S.L. McCracken, J.K. Tatman, Prediction of Ductility-Dip Cracking in Narrow Groove Welds Using Computer Simulation of Strain Accumulation, in: T. Boellinghaus, J.C. Lippold, C.E. Cross (Eds.), Cracking Phenomena in Welds IV, Springer International Publishing, Cham, 2016: pp. 119–141. https://doi.org/10.1007/978-3-319-28434-7_7.
[61] F. Christien, Role of Impurity Sulphur in the Ductility Trough of Austenitic Iron–Nickel Alloys, Materials. 13 (2020) 539. https://doi.org/10.3390/ma13030539.
[62] E.A. Torres, F. Montoro, R.D. Righetto, A.J. Ramirez, Development of high-temperature strain instrumentation for in situ SEM evaluation of ductility dip cracking, Journal of Microscopy. 254 (2014) 157–165. https://doi.org/10.1111/jmi.12128.
[63] EDF, “Code_Aster.” https://code-aster.org/
[64] A. Rapetti, Fissuration à chaud par chute de ductilité dans les métaux d’apport pour le soudage d’alliages à base de nickel, PhD Thesis, Université de Nantes, 2018. http://www.theses.fr/2018NANT4018/document.

[65] J. Bolivar, M. Frégonèse, J. Réthoré, C. Duret-Thual, P. Combrade, Evaluation of multiple stress corrosion crack interactions by in-situ Digital Image Correlation, Corrosion Science. 128 (2017) 120–129. https://doi.org/10.1016/j.corsci.2017.09.001.
[66] S. Mahalingam, P.E.J. Flewitt, J.F. Knott, The ductile–brittle transition for nominally pure polycrystalline nickel, Materials Science and Engineering: A. 564 (2013) 342–350. https://doi.org/10.1016/j.msea.2012.11.106.
[67] M. Yamaguchi, Grain Boundary Decohesion by Impurity Segregation in a Nickel-Sulfur System, Science. 307 (2005) 393–397. https://doi.org/10.1126/science.1104624.
[68] A. Larere, M. Guttmann, P. Dumoulin, C. Roques-Carmes, Auger electron spectroscopy study of the kinetics of intergranular and surface segregations in nickel during annealing, Acta Metallurgica. 30 (1982) 685–693. https://doi.org/10.1016/0001-6160(82)90118-3.